JOURNAL OF MATERIALS SCIENCE 32 (1997) 6207–6213

Formation of chloroaluminates in calcium aluminate cements cured at high temperatures and exposed to chloride solutions

M. A. SANJUÁN*
Department of Materials, Imperial College of Science, Technology and Medicine, London SW7 2BP, UK

The formation of hexagonal chloroaluminates in mortar specimens pre-cured at 20, 40 and 60 °C for two weeks and stored in a 0.5 M NaCl solution for up to 255 days has been studied. The appearance of this phase as a function of time has been monitored by X-ray diffraction. In addition, its microstructure has been observed by means of backscattering electron microscopy. The chemical composition was studied by X-ray microanalysis. The formation of chloroaluminate phases in reinforced concrete is related to the immobilization of chloride ions penetrating through the concrete to the reinforcement. Thus the formation of stable chloroaluminates could lower the risk of corrosion. In order to check this point, corrosion rate measurements were performed throughout the experiment. In spite of the high capacity of aluminous hydrates to react with chloride ions to form chloroaluminates, the remaining chloride ions in the pore solution leads over time to reinforcement corrosion. The presence of hexagonal phases in the cement paste ensure a better resistance against the penetration of chloride ions than when cubic phases are present. This effect was attributed to the denser microstructure exhibited, by samples containing the hexagonal phases.

1. Introduction

Calcium aluminate cements (CAC) were developed at the beginning of this century as a solution to the decomposition of Portland cements by sulphate attack. Its other properties, such as its high early strength and an excellent performance at high temperatures, make it a good material for precasting and refractory applications [1, 2].

Several different types of structural failures under various conditions have been reported in the literature [3–8]. The failures experienced with CAC have been attributed in some cases to a loss of strength due to reinforcement corrosion enhanced by the easier ingress of external aggressive agents in the more porous converted material. In consequence, the possibility of chloride attack cannot be ruled out.

Hexagonal crystals of CAH_{10} ($CaO \cdot Al_2O_3 \cdot 10H_2O$) and C_2AH_8 ($2CaO \cdot Al_2O_3 \cdot 8H_2O$) spontaneously convert to the cubic form [9–11]. This results in an increase in the porosity of the paste with an associated decrease in the resistivity of the pore solution, but no effect on the pH is observed [12]. This porosity change produces an easier access for external aggressive agents and allows them to penetrate into the sample and reach the reinforcement. In this paper this process has been speeded up by the application of heat (40 and 60 °C for 14 days).

An increasing interest has been shown about the ability of CAC to retard or even avoid the corrosion of the concrete reinforcement. This is thought to be a function of the formation of chloroaluminate compounds that can immobilize chloride ions that have penetrated from the external environment. Both the formation and stability of these compounds are relevant in determining the extent of the chloride ion corrosion process.

Salts are formed by the reaction between the penetrating chloride ions and the calcium aluminate cement. The structure of the chloroaluminates formed (Friedel's salt: $[Ca_2Al(OH)_6]Cl \cdot 2H_2O$ or $C_3A\ CaCl_2 \cdot 10H_2O$) consists of alternate slices of $Al(OH)_6$ octahedra distributed in a hexagonal net and connected by Ca atoms with an interlayer of composition $[Cl \cdot 2H_2O]^-$. The chlorine atoms form an hexagonal net of regular triangles with water molecules at their centre [12–14].

The aim of this paper is to investigate the possible formation of chloroaluminates in reinforced cementitious materials that are stable over the time period of the experiments and any possible influence of the chloroaluminates on the corrosion of steel reinforced fully converted samples.

2. Experimental procedures

Mortar specimens of size $20 \times 55 \times 80\ mm^3$, with a 1 : 2 water–cement and 1 : 3 cement–sand ratios were made.

* *Present address*: Instituto de Ciencias de la Construcción "Eduardo Torroja" – C/Serrano Galvache, s/n – 28.033 Madrid, Spain.

TABLE I Chemical composition of the calcium aluminate cement (wt %)

SiO_2	Al_2O_3	Fe_2O_3	FeO	CaO	MgO	SO_3	S	TiO_2	Cl	Na_2O	K_2O
4.5	39.0	12.0	4.0	38.5	0.6	0.15	0.02	2.5	0.01	0.10	0.15

The composition of the calcium aluminate cement (CAC) used is given in Table I. The sand grading ranged between 0–2 mm and distilled water was used. The specimens were cast under laboratory conditions. They were removed from the moulds after 24 h and then cured at 100% relative humidity (RH) and three temperatures of 20, 40 and 60 °C for 14 days, in order to obtain various degrees of conversion from hexagonal to cubic phases. Finally, they were stored at the laboratory temperature in a 0.5 M NaCl solution for 255 days.

2.1. X-ray diffraction

Sections of samples stored for 170 and 255 days were crushed and sieved to a fine powder for X-ray diffraction analysis. A plastic cap was used to remove most of the sand grains. A Philips PW1710 diffractometer equipped with a graphite monochromator and Cu$K_{\alpha 1}$ radiation was used over a 2θ angular range of 5–65°, with a step size of 0.04° at 2 s per step.

2.2. Sample preparation and electron microscopy analysis

Polished sections of the mortar samples were prepared for scanning electron microscopy (SEM) examination. After 255 days of storage, half of each specimen was cut longitudinally to the rebar for microstructural examination. Sections were then cut transversally to the steel rebar, resin impregnated, lapped with 9 μm alumina powder and polished from 3 to 0.25 μm to obtain a flat surface. The samples were then coated with carbon.

A JEOL JMS35-CF scanning electron microscope equipped with secondary and backscattered electron detectors, and also a Link System AN10000 energy dispersive X-ray spectrometer (EDS) was operated at an accelerating voltage of 15 keV in these experiments. X-ray microanalysis was performed on polished sections in the region of the steel/mortar interface using an energy dispersive detector, with the objective of investigating the presence of chloride ions either as Friedel's salt or as unbound species. The analyses were corrected using the ZAF procedure. This is a technique for quantitative analysis of flat polished specimens. In addition, an X-ray dot map was made of a section of the interfacial area to indicate the relative concentrations of Ca, Al, Fe and Cl.

2.3. Electrochemical measurements

Two steel bars were embedded in the mortar as twin working electrodes while a graphite rod was embedded mid-way between them to act as an auxiliary electrode. The steel bars had a 6 mm nominal diameter and had been previously cleaned in a 1:1 water–HCl solution containing 3 g l^{-1} of hexametilentetramine (a corrosion inhibitor), rinsed in acetone, dried and then weighed. Their ends were covered with a plastic insulating tape leaving an exposed area of 575 mm^2 in the middle.

The steel rebars were electrochemically monitored for ten months. The corrosion rate measurement (I_{corr}) of the embedded steel electrodes were obtained from polarization resistance measurements, R_p [15]. An Amel model 2053 potentiostat with electronic compensation of the ohmic drop (R_{ohm}) between the reference and working electrodes was used. A polarization sweep from −10 to 10 mV about the corrosion potential (E_{corr}) value was applied to the steel electrodes at a rate of 10 mV min^{-1} to measure the R_p value. The I_{corr} value was calculated assuming values of B (constants depending on the Tafel's slopes [15]) equal to 26 mV for the corroding steel and 52 mV for passive using Equation 1:

$$I_{corr} = \frac{\Delta I}{\Delta E} B = \frac{B}{R_P} \quad (1)$$

Corrosion rate values between 0.1–0.2 μA cm^{-2} are considered as the threshold between passivation and active corrosion. The corrosion potentials (E_{corr}) were measured with a calomel reference electrode.

3. Results

3.1. X-ray diffraction

X-ray diffraction patterns of the samples after 170 and 255 days of storage for the three different curing temperatures of 20, 40 and 60 °C for 14 days are shown in Figs 1 and 2. The X-ray diffraction patterns indicated the presence of Friedel's salt ($C_4ACl_2H_{10}$). No anhydrous compounds were recorded and they were probably removed by the sieving. The intensity of the peaks corresponding to the hexagonal phase CAH_{10} decrease as the temperature increased from 20 to 60 °C; whereas the peaks corresponding to Friedel's salt ($C_4ACl_2H_{10}$) increase. On the other hand, C_2AH_8 was not detected, and thus the formation of this phase can be assumed to be negligible at 20, 40 and 60 °C. In practice, this compound is the dominant phase in the range around 30–35°C, but is almost absent at temperatures above and below it.

Fig. 3 shows the X-ray diffraction patterns of the specimen that was not exposed to the chloride solution thereby allowing comparisons with the exposed samples. It can be observed that no $C_4ACl_2H_{10}$ is present, whereas the same trend is observed in the case of the hexagonal CAH_{10} cubic C_3AH_6, and γ-AH_3 phases.

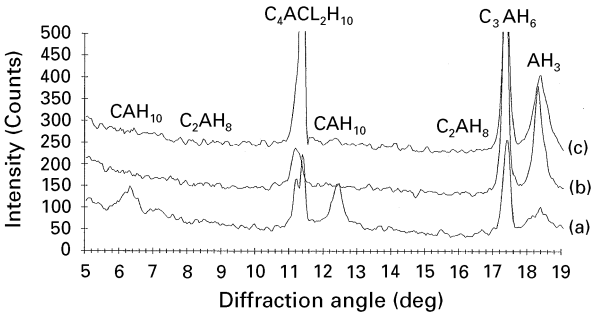

Figure 1 X-ray diffraction patterns of samples aged for 170 days in a 0.5 M NaCl solution, after a 14 day annealing at: (a) 20 °C; (b) 40 °C and (c) 60 °C.

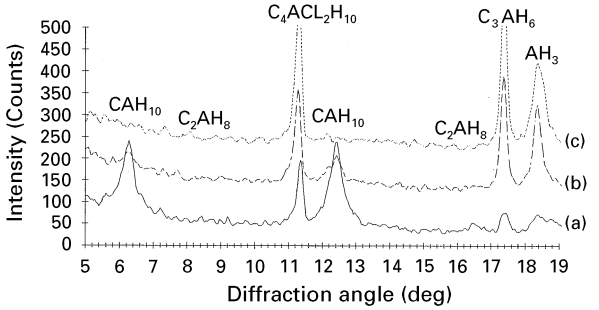

Figure 2 X-ray diffraction patterns of samples aged for 255 days in a 0.5 M NaCl solution after a 14 day annealing at: (a) 20 °C; (b) 40 °C and (c) 60 °C.

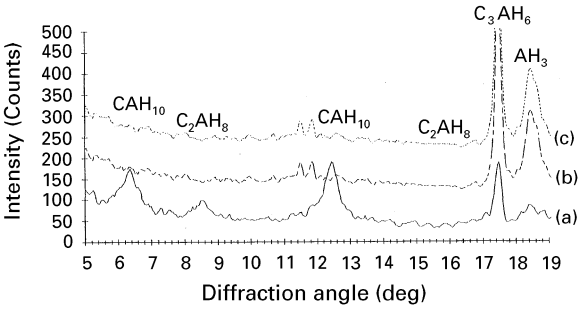

Figure 3 X-ray diffraction patterns of the reference samples (no chloride exposure) (a) 20 °C; (b) 40 °C and (c) 60 °C.

3.2. Electron microscopy analyses

Using back-scattered electron (BSE) techniques it was possible to recognize Friedel's salt existing as well formed plates either close to the steel bar or inside the mortar when the specimen was precured at 60 °C. Friedel's salt could sometimes be observed in the 40 °C sample and only rarely in the 20 °C sample. In the latter sample Friedel's salt $C_4ACl_2H_{10}$ was never observed close to the steel. These conclusions were undefined by the X-ray diffraction. The X-ray micro-analysis of regions of $C_4ACl_2H_{10}$ plates gave Cl/Al ratios slightly below the theoretical value of 1. This fact explains a small observed shift in the diffraction peak positions in the X-ray diffraction patterns.

BSE micrographs of the mortar specimen and the mortar–steel interface are shown in Figs 4 and 5, respectively. The chloroaluminate appears as hexagonal plates in both cases forming clusters as large as 30 μm.

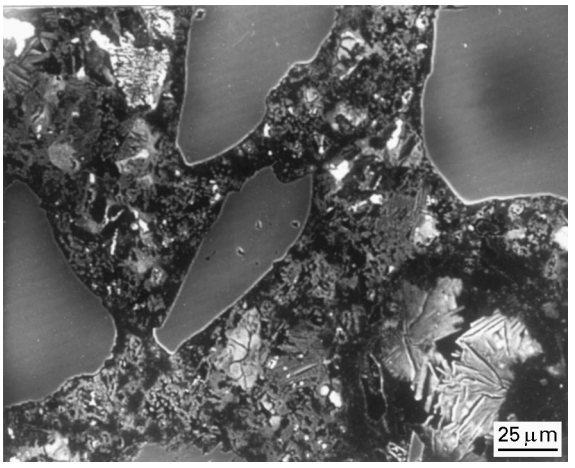

Figure 4 BSE micrograph in the mortar specimen cured at 60 °C showing $C_4ACl_2H_{10}$ plates.

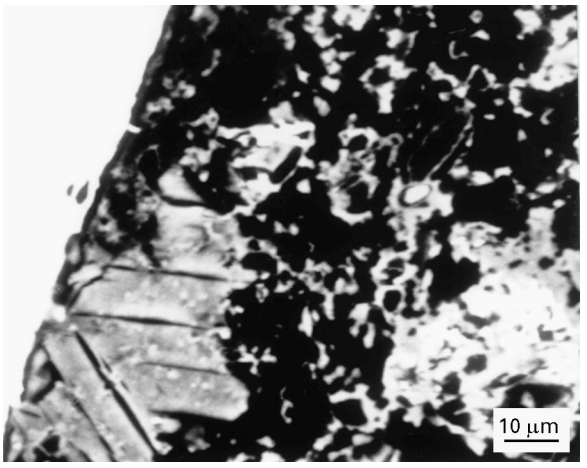

Figure 5 BSE micrograph of the mortar–steel interface of the specimen cured at 60 °C.

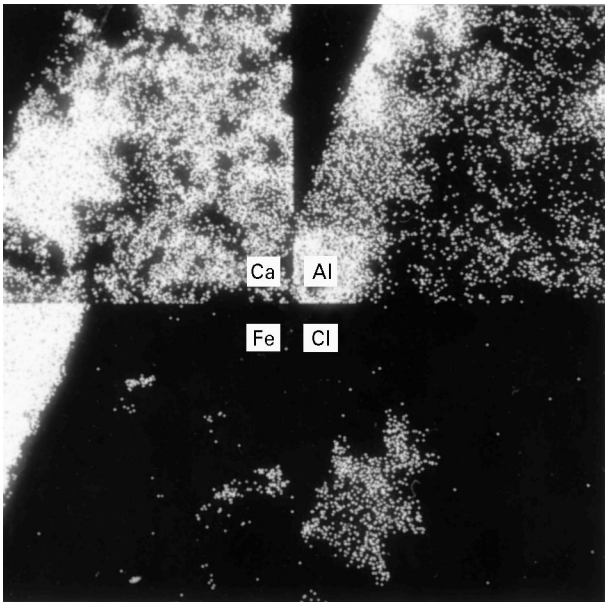

Figure 6 X-ray dot map analyses showing the distribution of Ca, Al, Fe and Cl in the interface with the steel.

They grow preferentially in voids which exist in the mortar and also close to the rebar.

X-ray dot map analyses were performed, Fig. 6, in order to assess the distribution of Ca, Al, Fe and Cl

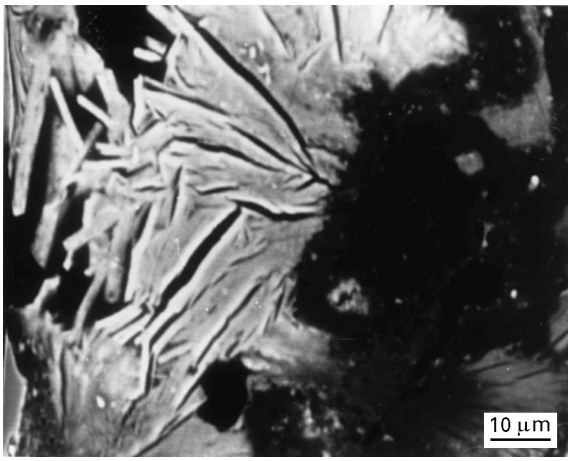

Figure 7 BSE micrograph a Friedel's salt compound.

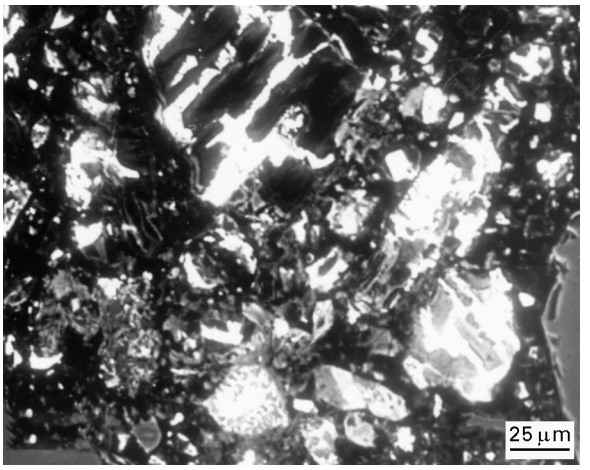

Figure 9 BSE micrograph of a sample stored in the 0.5 M NaCl solution after curing at 20 °C.

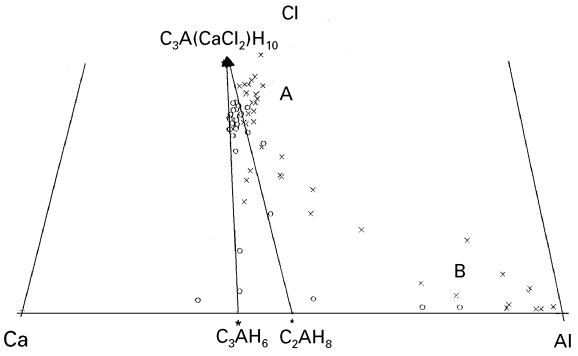

Figure 8 Ternary phase diagram for Cl–Al–Ca. Key: (×) inside the sample and (○) near the steel.

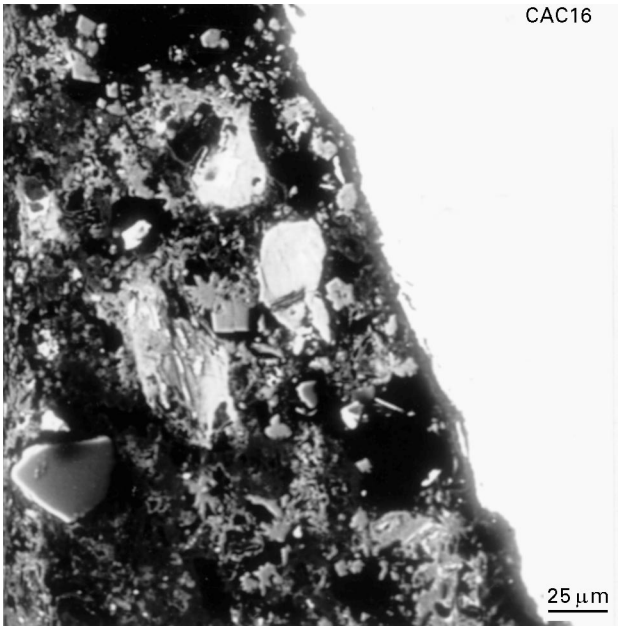

Figure 10 BSE micrograph of a sample stored in the 0.5 M NaCl solution after curing at 40 °C.

in the mortar and the mortar–steel interfacial areas in which calcium aluminates appeared in the specimen cured at 60 °C and stored in a 0.5 M NaCl solution. Chloroaluminates are clearly identified using this technique by means of the coincidence in the respective windows of a high concentration of Cl, Ca and Al. These observations were confirmed by point X-ray microanalyses.

Fig. 7 shows a typical Friedel's salt formation on which X-ray dot map analysis was performed. Fig. 8 shows the ternary phase diagram for Cl–Al–Ca obtained as the result of the point analyses taken on chloroaluminates found close to the steel and inside the bulk sample. The close agreement between the composition given by the point analysis for the hexagonal plates and that of the Friedel's salt ($C_4ACl_2H_{10}$) should be noted.

CAH_{10} (hexagonal) was the only hydration product detectable by X-ray diffraction in any of the specimens examined, which was partially converted into C_3AH_6 (cubic) plus γ-AH_3. CAH_{10} had the appearance of small prisms whereas the C_3AH_6 seemed to be an array of nodules surrounded by amorphous γ-AH_3. This γ-AH_3 was observed as an amorphous region of dark grey level all around the Friedel's salt and aggregates. In spite of being a poorly crystalline phase it has been possible to detect it by means of X-ray diffraction. C_2AH_8 was not observed by BSE in any of the cases studied.

For comparison, Figs 9 and 10 show micrographs corresponding to the samples stored in the 0.5 M NaCl solution after curing at 20 and 40 °C, respectively. The BSE images showed that, after 2 weeks of being cured at 20 °C, the microstructure consists mainly of CAH_{10} prisms together with pores. The 40 °C cured mortar showed a marked change in microstructure as result of the conversion of this phase into C_3AH_6 and γ-AH_3, confirmed by X-ray diffraction, which resulted in the observation of highly porous regions separated by relatively dense regions. Also, a great contrast in the microstructure between both samples is observed with distance from the steel. At the interface, a very high porosity was detectable in the BSE images for the sample cured at 40 °C. The changes observed with distance from the edge of the specimens is attributed to temperature gradients within the specimen. The combined use of BSE and X-ray diffraction allows a deeper understanding of the hydration products of CAC to be obtained.

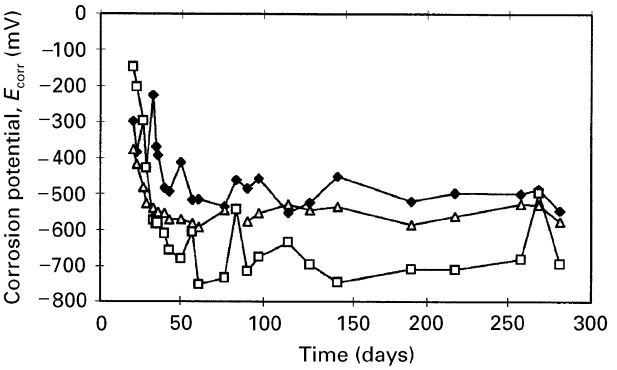

Figure 11 The corrosion potential as a function of the time the samples were stored in the 0.5 M NaCl solution after curing at temperatures of: (◆) 20 °C; (□) 40 °C and (△) 60 °C.

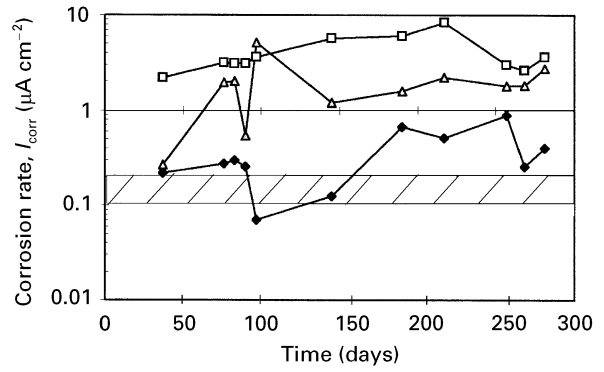

Figure 12 The corrosion rate as a function of the time the samples were stored in the 0.5 M NaCl solution after curing at temperatures of: (◆) 20 °C; (□) 40 °C and (△) 60 °C.

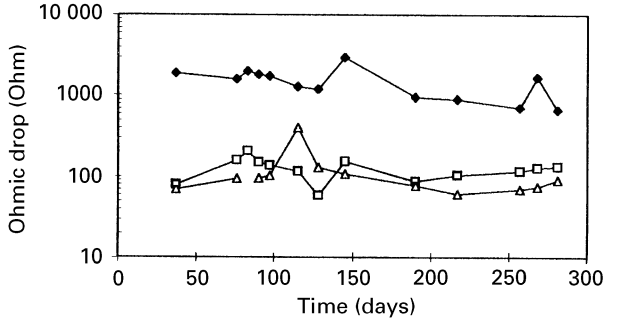

Figure 13 The ohmic drop as a function of the time the samples were stored in the 0.5 M NaCl solution after curing at temperatures of: (◆) 20 °C; (□) 40 °C and (△) 60 °C.

3.3. Electrochemical measurements

Corrosion potentials as a function of storage time are shown in Fig. 11 for samples cured at 20, 40 and 60 °C. The observed sharp decrease in the corrosion potential is evidence of the penetration of chloride ions through the mortar. The smallest drop was detected in the specimens cured at 20 °C. However, all three samples showed a very negative E_{corr} ranging between -500 to -800 mV. Corrosion rate results (Fig. 12) showed an acceptable performance of the steel bars embedded in the mortar cured at 20 °C over the first 150 days ($I_{corr} < 0.2$ μA cm^{-2}); whereas those cured at 40 and 60 °C showed corrosion rates over 1 μA cm^{-2}.

The dashed zone in Fig. 12 shows the boundary between significant corrosion (high corrosion rates over 0.2 μA cm^{-2}) and low corrosion [15].

With regard to the ohmic drop of these specimens which is evidence of a dependence on the microstructure of the cement paste: the higher the ohmic drop the more dense the material as is the case for the hexagonal phases (20 °C curing) and a lower ohmic drop is associated with the less dense cubic phases (40 and 60 °C curing).

4. Discussion

A transformation of hexagonal aluminates to cubic ones via dissolution can occur in the samples [10]. The main hydrated phase produced at 20 °C is the hexagonal CAH_{10}, which is metastable and over time it tends to convert into the thermodynamically more stable cubic C_3AH_6 phase. A high curing temperature promotes this conversion and the results obtained were as expected. The conversion of the tested samples has been observed by X-ray diffraction with the specimens cured for 14 days at 40 and 60 °C, showing a total conversion (Fig. 1). This resulted in increased sample porosity and thus an easier path for the ingress of chloride ions [4] which in turn leads to significant chloroaluminates formation in these samples as compared to the one cured at 20 °C. The detected small shift of the basal spacing detected in the X-ray patterns is due to the increasing replacement of OH^- by Cl^- [16].

It has been reported that calcium chloroaluminate can appear in paste samples made with 3 wt % NaCl in the mixing water [17]. This phase seems to be unstable and disappears with time enhancing the cubic C_3AH_6 formation [18]. In contrast, a high concentration of chloroaluminates still remains after 255 days of testing under the present experimental conditions. The stability of this compound seems to be influenced by other factors apart from the pH of the pore solution because it is not significantly changed by the conversion process [12]. In the presence of chlorides a small increase in the pH is recorded [18]. The penetration of chloride ions results in an increase in the pore solution pH because hydrates bind the chloride leaving OH^-. However, the presence of sodium ions affects the equilibrium in the pore solution and enhances the conversion.

Friedel's salt was detected using X-ray diffraction techniques in all the specimens that had been exposed to the chloride solutions. Its relative amount depended on the degree of conversion of the hexagonal phase to cubic phase. Specimens cured at 60 °C had higher concentrations of Friedel's salt as result of a higher chloride concentration that had penetrated the material due to its higher porosity. In contrast, when the chloride is added to the mixing water samples that are cured at higher temperatures less amounts of Friedel's salt are produced than in the samples cured at lower temperatures [21].

The formation of chloroaluminates has been defined as a replacement of OH^- in the hexagonal CAH_{10} phase by chloride ions in a solid solution.

However, this paper shows using the X-ray diffraction data of Fig. 1 that the appearance of this compound in calcium aluminate cement occurs after the hexagonal phase has been converted to the cubic phase. In this case, the formation of chloroaluminates is thought to involve the cubic phases C_3AH_6.

On the other hand, the loss of strength attributed to the conversion process [6], does not directly affect the reinforcement corrosion [17, 19]. Only an increase in porosity and water content in the pores is detected. Thus, the conversion process by itself is not able to initiate the reinforcement corrosion. Therefore, the easier access routes for the external aggressives to penetrate into the mortar is the factor that enhances the risk of corrosion after conversion. In chloride contaminated environments only the ingress of chloride ions through the mass of the concrete and the ability of the cementitious matrix to immobilize the chloride ions affects further initiation of corrosion. The good resistance of calcium aluminate paste to chloride solutions was attributed to the formation of a protective layer [20] in addition to the great potential for chloride binding by chloroaluminate formation. These facts apparently make CAC more protective to steel than normal Portland cement.

Friedel salt decomposition and subsequent chloride liberation into the pore solution has been postulated to explain the initiation of the corrosion [18]. Nevertheless, the present results suggest that chlorides replace OH^- groups linked to Al^{3+} in the mortar forming chloroaluminates but that sufficient chloride remains in the pore solution to initiate corrosion.

The low I_{corr} values previously reported in the literature [18] can be explained by the point that chloride activity when added to the mixing water is less aggressive than chloride penetrating from the external environment. However, recently high I_{corr} values have been reported in the literature in similar conditions [21]. These apparently contradictory results suggest that laboratory tests performed by adding chloride to the paste to accelerate the experiments do not adequately reflect structures placed in marine environments.

The higher chloride binding capacity of CAC with respect to ordinary Portland cement is believed to be due to the point that it does not significantly influence the corrosion initiation when the material is in contact with a continuous external source of chlorides such as sea water. In contrast to previous reports in the literature [21] where high corrosion rates are attributed to bad practice, the results presented here demonstrate that high corrosion rates are to be expected when a highly porous mortar or concrete is exposed to chlorides. Thus, the corrosion rate mainly depends on the porosity of the material which results in the easier movement of external aggressives into the mortar.

The difference in ohmic drop behaviour is related to the different types of microstructures observed in the samples: hexagonal plates leading to a more dense material while cubic hydrates produced a less dense material. It is thought that the conversion process occurred during the first two weeks of curing, before they were immersed in the salt solution. Thus such differences cannot be attributed to water liberated during the conversion as has been previously suggested [18], this is believed to be due to a different porous microstructure. However, these results agree with the suggestion that this technique can be used to characterize the conversion process in CAC samples.

5. Conclusion

Reinforced mortar specimens cured for 14 days at 40 and 60 °C showed total conversion and the chloroaluminate phase was present. This suggests the participation of the cubic phase in generating the Friedel's salt. This compound was observed in samples immersed in salt solution for 177 and 255 days thereby demonstrating its potential for immobilizing chloride ions. Further work is necessary to assess the stability of this system. With regard to the reinforcement corrosion it can be stated that aluminate hydrates can partly immobilize the chlorides, although over time the threshold level to initiate corrosion is reached. The important parameter in determining corrosion initiation is the open porosity of the material.

Acknowledgements

MAS wishes to thank the Directorate-General for Science, Research and Development of the European Commission for the receipt of a Fellowship under the Human Capital and Mobility programme. The author also thanks K. L. Scrivener and H. Fryda for comments and help during the work and Cements Lafarge for supplying the CAC. A special acknowledgement to my colleagues N. Constantinou, M. Lewis, S. Laing, S. Jensen, L. Achimastos, J. Houghton and S. Wang.

References

1. C. M. GEORGE, *Revue des Materiaux de Construction* **4** (1976) 201.
2. A. NEVILLE, *Il Cemento* **3** (1978) 291.
3. D. BRIESEMANN, *Betonstein-Zeitung* **10** (1969) 593.
4. D. C. TEYCHENNÉ, *Mag. Concr. Res.* **27** (1975) 78.
5. A. NEVILLE, "High Alumina Cement Concrete" (The Construction Press Ltd, Lancaster, 1975).
6. M. PÉREZ, T. VÁZQUEZ and F. TRIVIÑO, *Cem. Concr. Res.* **13** (1983) 795.
7. S. C. C. BATE, "High Alumina Cement Concrete in Existing Building Superstructures" (Building Research Establishment, Watford, UK, 1984).
8. R. J. COLLINS and W. GUTT, "Update on Assessment of High Alumina Cement Concrete" (Building Research Establishment, Watford, UK, 1988).
9. P. K. METHA and G. LESNIKOFF, *J. Amer. Ceram. Soc.* **52** (1971) 210.
10. P. BRADBURY, P. CALLAWAY and D. D. DOUBLLE, *Mater. Sci. Engng.* **23** (1976) 43.
11. H. G. MIDGLEY, *Mag. Concr. Res.* **27** (1975) 59.
12. M. T. GAZTAÑAGA, Tesina de Licenciatura. Facultad de Ciencias Químicas. Universidad Complutense de Madrid (1989).
13. S. J. AHMED, L. S. DENT GLASSER and H. F. W. TAYLOR, in Proceedings of the Fifth International Symposium on the Chemistry of Cement. Tokyo, 1968, pp. 118–127.

14. A. TERZIS, S. FILIPPAKIS, H-J. KUZEL and H. BURZLOFF, *Z. Krist.* **181** (1987) 29.
15. C. ANDRADE and J. A. GONZÁLEZ, *Werkst. Korros.* **29** (1978) 515.
16. W. DOSCH, H. KELLER and H. ZUR STRASSEN, in Proceedings of the Fifth International Symposium on the Chemistry of Cement. Tokyo, 1968, pp. 118–127.
17. S. GOÑI, C. ANDRADE and C. L. PAGE, *Cem. Conr. Res.* **21** (1991) 635–646.
18. S. GOÑI, M. T. GAZTAÑAGA, J. L. SAGRERA and M. S. HERNÁNDEZ, *J. Mater. Res.* **9** (1994) 1533.
19. M. PÉREZ, F. TRIVIÑO and C. ANDRADE, *Materiales de Construcción* **182** (1981) 49.
20. G. M. DARR and U. LUDWIG, *Ind. Chim. Belg.* **39** (1974) 687.
21. A. MACÍAS, A. KINDNESS and F. P. GLASSER, *J. Mater. Sci.* **31** (1996) 2279.

Received 10 March
and accepted 28 April 1997